

# Rethinking LayerNorm in Image Restoration Transformers

MinKyu Lee, Sangeek Hyun, Woojin Jun, Hyunjun Kim, Jiwoo Chung, Jae-Pil Heo\*  
Sungkyunkwan University

{2minkyulee, hse1032, junwoojinjin, arithu3, jiwoo.jg, jaepilheo}@gmail.com

## Abstract

This work investigates abnormal feature behaviors observed in image restoration (IR) Transformers. Specifically, we identify two critical issues: feature entropy becoming excessively small and feature magnitudes diverging up to a million-fold scale. We pinpoint the root cause to the per-token normalization aspect of conventional LayerNorm, which disrupts essential spatial correlations and internal feature statistics. To address this, we propose a simple normalization strategy tailored for IR Transformers. Our approach applies normalization across the entire spatio-channel dimension, effectively preserving spatial correlations. Additionally, we introduce an input-adaptive rescaling method that aligns feature statistics to the unique statistical requirements of each input. Experimental results verify that this combined strategy effectively resolves feature divergence, significantly enhancing both the stability and performance of IR Transformers across various IR tasks.

## 1. Introduction

Image restoration (IR) is a fundamental challenge in computer vision that aims to reconstruct high-quality images given degraded ones, including tasks such as image super-resolution (SR), image denoising (DN), and JPEG image compression artifact removal (CAR) and Deraining (DR). With the emergence of deep learning techniques, there has been significant progress in accurately restoring images, surpassing earlier signal processing-based methods.

With the success of Vision Transformers [8] in a variety of computer vision tasks, numerous efforts have been made to adapt the Transformer architecture also for image restoration tasks. In particular, Transformer-based architectures such as SwinIR [16] has been emphasized due to their significance against CNNs. Accordingly, the Transformer-based architecture has become the standard macro design in recent IR networks, which consists of consecutive attention and feed-forward layers, together with residual connections and normalization layers each.

\*Corresponding author.

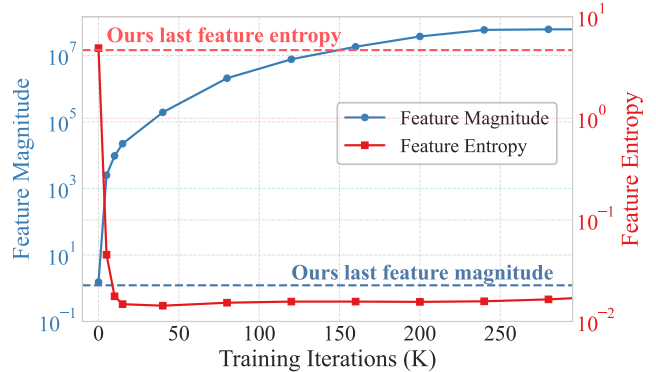


Figure 1. Evolution of feature magnitudes and channel-axis feature entropy during training an Image Restoration (IR) Transformer using conventional (per-token) LayerNorm. Along with this, we show the final values of magnitude and entropy of IR Transformer features when trained with our proposed *i*-LN (dashed lines). With conventional LayerNorm, feature magnitudes diverge dramatically to a million-scale, accompanied by a sharp decline in channel-axis entropy. This indicates highly concentrated (peaky) distributions in specific channels, potentially limiting the performance. In Sec. 4.2, we demonstrate that this phenomenon arises as the network attempts to bypass LayerNorm’s constraints, which neglect crucial aspects of IR tasks such as spatial consistency and input-dependent feature statistics. In contrast, our proposed *i*-LN maintains stable feature magnitudes and entropy levels, reflecting well-distributed channel activations and healthy training dynamics.

Notably, most of these IR Transformers employ LayerNorm [2], which normalizes each token independently. Despite improvements in enhancing the functionality of the attention mechanism and the feed-forward layers, the empirical impact of this per-token operation in LayerNorm for IR tasks has been largely overlooked.

Meanwhile, we observe an interesting phenomenon in IR Transformers across various IR tasks, where the feature magnitude exhibits abnormal behavior. Under conventional LayerNorm, the squared feature norms diverge up to a million scale while feature entropy along the channel-axis drops sharply (Fig. 1), driven by concentration of peaky values in specific channels (Sec. 4.2).

Inspired by these observations, this work addresses the abnormal feature behavior and the potential performance

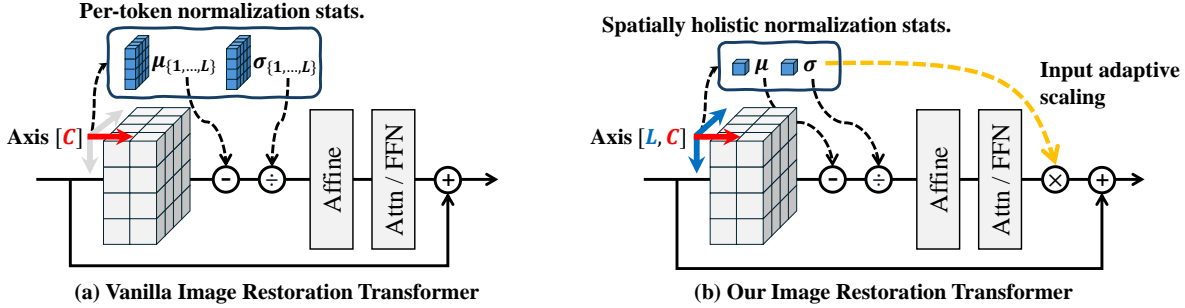


Figure 2. Basic Transformer blocks with vanilla LayerNorm (LN) and the proposed Image Restoration Transformer Tailored LayerNorm (*i*-LN). We normalize based on the entire spatio-channel dimension of internal features instead of handling each token individually. Additionally, we rescale the feature post attention and feed-forward networks based on the normalization statistics. Together, our approach enables us to preserve the internal spatial correlation and align feature statistics with the unique requirements for different input patterns.

limit by focusing on: 1) spatial consistency in normalization and 2) input dependency of internal feature statistics; which are aspects often overlooked in prior works.

Initially, we analyze the underlying training dynamics of IR Transformers and establish connections between the feature divergence phenomena and the usage of LayerNorm. We tackle the per-token normalization scheme of typical LayerNorm in Transformers which disrupts spatial relationships. Since preserving this spatial correlations among features is essential for high-fidelity image restoration, we hypothesize that networks attempt to bypass the per-token normalization by sneaking amplified values in specific channels that dominate the feature statistics. Such adaptations result in the divergence of intermediate feature magnitudes, potentially degrading the overall performance and stability of the restoration process.

In this work, we demonstrate that this divergence can be addressed in a surprisingly straightforward manner. We propose to normalize features across the entire spatio-channel dimension rather than normalizing each token independently in IR Transformers, as shown in Fig.2. This approach allows us to normalize features in a more holistic and coherent manner without disrupting the original spatial relationships. Consequently, the network no longer needs to introduce abnormal values to circumvent per-token normalization constraints in order to preserve spatial relationships.

Additionally, we further tailor normalization for image restoration tasks to accommodate the input dependency of intermediate feature statistics. Unlike many downstream tasks that aim to transform images into a uniformly normalized feature space, the internal and output image statistics in image restoration can vary significantly depending on the input image patterns. Given that standard normalization techniques often overlook this variability, we aim to maintain internal feature statistics by rescaling features with the normalization parameters after each attention or feed-forward layer. This tailored approach ensures that the intermediate features accommodate the unique statistical char-

acteristics of each input image, enhancing both the effectiveness and precision of the restoration process. Throughout this work, we will refer to this as the Image Restoration Transformer Tailored Layer Normalization, or simply *i*-LN.

Extensive experiments validate that by substituting conventional LayerNorm with *i*-LN, we can effectively stabilize feature magnitudes and preserve the intrinsic spatial correlations essential in IR Transformers. Additionally, we can achieve substantial performance improvements across various image restoration tasks and also obtain an IR Transformer that is friendly to reduced-precision inference.

**Remarks.** Our goal is to explore the internal training dynamics of IR Transformers and provide a comprehensive analysis, rather than achieving state-of-the-art performance on specific IR tasks. Consequently, we keep the overall method simple and propose a straightforward architecture that effectively addresses the issues identified in our observations. We leave the exploration of more complex architectures designed for peak performance for future studies.

## 2. Related Work

**Image Restoration Transformers** Recent advances in Image Restoration (IR) transformers archive superior performance over CNNs by leveraging attention mechanisms to effectively model long-range context. A pioneering work, SwinIR [16], adopted efficient Swin-Transformer [19] based architecture in IR tasks, balancing computational cost and restoration quality. Restormer [27] introduced multi-scale channel-wise attention, enhancing feature learning for IR tasks through improved cross-scale dependency modeling. A notable method is HAT [5, 6], which originated as a super-resolution model but expanded to general image restoration tasks. By unifying spatial and channel attention within a hybrid attention framework, HAT surpasses existing IR Transformers in both restoration fidelity and robustness across various IR tasks. Building on these advancements, we adopt the representative IR transformers, SwinIR and HAT, as the backbone architecture for our method.

**Abnormal Feature Behaviors in Deep Networks** Normalization is a key element in enhancing stability and performance in deep networks, but also can lead to unintended feature behavior. EDSR [18], which is a foundational work in super-resolution pointed out that BatchNorm removes range flexibility of intermediate features leading to performance drop. Accordingly, normalization layers are removed in most recent CNN-based SR architectures. Meanwhile, ESRGAN [24] and StyleGAN2 [14] observe that InstanceNorm and BatchNorm, respectively, causes water droplet-like artifacts. They suggest that the generator might learn to deceive feature statistics by sneaking abnormal values in internal features to reduce the effects of normalization. EDM2 [15] identifies feature magnitude divergence in diffusion models. Accordingly, they redesign the network architecture to preserve the magnitude based on statistical assumptions, leading to overall performance enhancement. DRCT [11] notes that feature map intensities drop sharply at the end of SR networks, finding that addressing abnormal feature scale may lead to improved performance.

### 3. Method

#### 3.1. Observation

**Abnormal Feature Statistics** Our initial analysis focuses on tracking the trajectory of internal feature scales during the training of IR Transformers. Following the conventions [15], we visualize the squared mean of intermediate features at each basic building block of the network. We select the x4 SR task using the representative HAT model, specifically analyzing the output of each building block throughout the training progression.

The analysis reveals that feature statistics diverge dramatically, reaching values up to a *million* scale, and furthermore, we observe that this phenomenon occurs regardless of IR tasks (Fig.3). Since these extreme values are unusual, this motivates us for further investigation. To pinpoint the origins of this feature divergence, we analyze the feature entropy across the channel axis of the last block where the feature divergence is most severe. We observe a gradual decrease in feature entropy, which indicates the presence of peaky channels that dominate the statistics.

Notably, this type of abnormal peaky values hidden across the channel dimension aligns with the findings in prior studies [14, 24, 25], which have discussed how neural networks sneak peaky values to bypass normalization.

Inspired by prior observations, we identify the root cause of this feature divergence as LayerNorm, commonly used in conventional IR Transformers. We narrow down the origin of the feature divergence as: 1) the per-token normalization scheme, which disrupts spatial correlations of intermediate features, and 2) the input-blind mapping of LayerNorm, which maps any input patch into a unified normalized space, disregarding the unique statistical properties of

the input pattern.

Overall, since LayerNorm neglects important requirements of intermediate features that are crucial when solving image restoration tasks, the network amplifies values in specific channels that dominates the feature statistics, thereby effectively circumventing the inadequate constraints of LayerNorm.

#### 3.2. Tailoring LayerNorm for IR Transformers

**Vanilla LayerNorm (LN)** In Transformer architectures, the LayerNorm is the de facto normalization scheme. Originating from Natural Language Processing tasks, it normalizes each token independently. Specifically, it manipulates the statistics in a per-token manner as follows:

$$\mu_l = \mathbb{E}_c[x_{l,c}], \quad \sigma_l^2 = \mathbb{E}_c[(x_{l,c} - \mu_l)^2], \quad (1)$$

$$\text{LayerNorm}(x_l) = \gamma \frac{1}{\sqrt{\sigma_l^2 + \epsilon}} (x_l - \mu_l) + \beta, \quad (2)$$

where  $x_l \in \mathbb{R}^C$  are tokens from each spatial location and the expectation  $\mathbb{E}_c[\cdot]$  is taken over the channel dimension  $c$ , and  $\gamma, \beta$  are each channel-wise affine transformation parameters. As discussed above, vanilla LayerNorm acts in a per-token manner, neglecting the spatial consistency and input dependency of internal feature statistics, leading to abnormal feature behaviors and suboptimal performance.

To address this issue, we propose the Image Restoration Transformer Tailored LayerNorm (*i*-LN), which manages to accommodate both the spatial consistency and input dependency within the normalization scheme. Later, we provide extensive experimental results validating the effectiveness of *i*-LN, which leads to well-bounded intermediate feature scale and also substantial performance improvement across various IR tasks.

##### 3.2.1. IR Transformer Tailored Normalization

**Spatially Holistic Normalization** We propose a simple variant of LayerNorm that preserves the spatial relationships between tokens. Specifically, instead of computing normalization statistics for each token individually, we derive them from the entire spatio-channel dimension of the feature, indicated as LN\*, as follows:

$$\mu = \mathbb{E}_{l,c}[x_{l,c}], \quad \sigma^2 = \mathbb{E}_{l,c}[(x_{l,c} - \mu)^2], \quad (3)$$

$$\text{LN}^*(x) = \gamma \frac{1}{\sqrt{\sigma^2 + \epsilon}} (x - \mu) + \beta, \quad (4)$$

where  $x_{l,c}$  is a  $c^{\text{th}}$  channel of  $l^{\text{th}}$  token in  $x \in \mathbb{R}^{L \times C}$ , and  $x$  is a set of tokens representing an entire image, and the expectation  $\mathbb{E}_{l,c}[\cdot]$  is taken over both spatial ( $l$ ) and channel dimensions ( $c$ ). This straightforward modification effectively mitigates the issue raised by the per-token operation

Backbone	Scale	Set5		Set14		BSD100		Urban100		Manga109	
		PSNR	SSIM								
HAT + LN [5]	×2	38.14	.9610	33.78	.9196	32.19	.9000	32.16	.9297	38.84	.9778
HAT + <i>i</i> -LN (Ours)	×2	<b>38.37</b>	<b>.9619</b>	<b>34.08</b>	<b>.9218</b>	<b>32.42</b>	<b>.9028</b>	<b>33.32</b>	<b>.9385</b>	<b>39.69</b>	<b>.9794</b>
DRCT + LN [11]	×2	38.19	.9613	33.28	.9197	32.28	.9010	32.60	.9323	39.23	.9785
DRCT + <i>i</i> -LN (Ours)	×2	<b>38.23</b>	<b>.9614</b>	<b>33.86</b>	<b>.9206</b>	<b>32.31</b>	<b>.9014</b>	<b>32.79</b>	<b>.9344</b>	<b>39.40</b>	<b>.9788</b>
HAT + LN [5]	×4	32.51	.8992	28.79	.7876	27.68	.7411	26.55	.8015	31.01	.9150
HAT + <i>i</i> -LN (Ours)	×4	<b>32.72</b>	<b>.9019</b>	<b>29.01</b>	<b>.7915</b>	<b>27.84</b>	<b>.7456</b>	<b>27.17</b>	<b>.8167</b>	<b>31.82</b>	<b>.9228</b>
DRCT + LN [11]	×4	32.50	.8989	28.85	.7871	27.73	.7414	26.63	.8021	31.24	.9169
DRCT + <i>i</i> -LN (Ours)	×4	<b>32.57</b>	<b>.8997</b>	<b>28.91</b>	<b>.7887</b>	<b>27.76</b>	<b>.7426</b>	<b>26.79</b>	<b>.8063</b>	<b>31.41</b>	<b>.9188</b>

Table 1. Quantitative comparison for **image super-resolution**. The best results for each setting are highlighted in **bold**, respectively.

in vanilla LayerNorm. It enables us to preserve the essential spatial correlations and thereby significantly alleviate the feature divergence phenomena.

**Preserving Internal Statistics** Apart from the improvements introduced above, we further tailor LayerNorm to suite the requirements in IR tasks. Here, we tackle the issue of input-blind normalization.

Unlike typical downstream tasks that embed images into a unified normalized feature space, IR tasks require preserving the low-level characteristics of input image patterns to accurately reconstruct them. However, conventional LayerNorm in IR Transformers neglect this issue and map intermediate features into a unified normalized space, neglecting the unique requirements in image restoration tasks. Accordingly, while normalization enhances training stability, it also causes the model to lose important input dependent characteristics and significantly limits the range flexibility.

Notably, these insights align with prior studies in CNN-based SR networks [18, 24], which has removed all normalization layers within the network architecture due to similar concerns. However, our observations indicate a clear failure in IR Transformers when normalization is completely omitted (Tab.5).

To this end, we propose a simple rescaling strategy that effectively tackles this issue. We rescale the output of attention and feed-forward networks by their standard deviation computed in the normalization process. Accordingly, a typical Transformer layer could be improved as follows:

$$\hat{x}^{i-1} = x^{i-1} + \sqrt{(\sigma^i)^2 + \epsilon} \cdot \text{Attn}(\text{LN}^*(x^{i-1})), \quad (5)$$

$$x^i = \hat{x}^{i-1} + \sqrt{(\hat{\sigma}^i)^2 + \epsilon} \cdot \text{FFN}(\text{LN}^*(\hat{x}^{i-1})), \quad (6)$$

where  $i$  is a block index and  $\sigma$  the a standard-deviation of features in eqn. 3. For simplicity, we denote the attention variants of IR Transformers (e.g., Windowed Multi-head Self-Attention of SwinIR, Overlapping Cross-Attention and Hybrid-Attention of HAT) simply as Attn, and also likewise for variants of feed-forward networks as FFN. Overall, this acts as an input dynamic scaling factor that enables us to

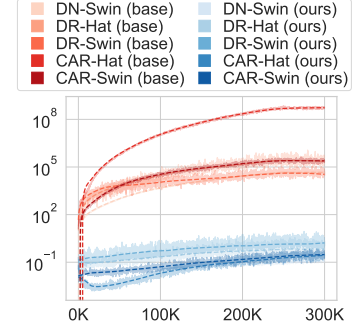


Figure 3. Feature divergence appears across various IR tasks.

align the internal feature statistics of IR Transformers with the unique requirements of each input pattern. Later, we will show that this simple strategy leads to substantial performance improvement.

## 4. Experiments

**Training Settings.** Since recent works are known to have discrepancy in their training settings [7], we reimplement and train both the baseline methods and our method in identical settings for fair comparison. We use Rain13K [13] to train Deraining networks, and DF2K to train networks for all other tasks, which is a combination of DIV2K [1] and Flickr2K [17]. We only use geometrical augmentations including random flips, rotations and crops. We do not use mixing augmentations, progressive learning (patch size), warm start-up (scale). The optimizer is Adam with learning rate  $2e-4$ , and networks are trained up to 300K iterations in all settings. We have limited the training patch size as  $128 \times 128$  for  $\times 4$  super-resolution (SR),  $64 \times 64$  for denoising (DN) and JPEG compression artifact removal (CAR) and  $\times 2$  SR,  $128 \times 128$  for Deraining (DR). We employ representative IR Transformers: SwinIR [16], HAT [5] and additionally DRCT [11].

**Evaluation Settings.** Standard benchmarks are employed including: Set5 [4], Set14 [28], BSD100 [20], Urban100 [12], Manga109 [21] for SR; CBSD68 [20], Kodak [10], McMaster [30], Urban100 for DN; LIVE1 [22], Classic5 [9], Urban100 [12] for CAR; Test100 [29] and Rain100L [26] for DR. Urban100 was cropped into non-overlapping  $256 \times 256$  sub-patches due to GPU memory limits for CAR and DN. We report PSNR and SSIM indices. For SR and DR, scores are evaluated in the Y of YcbCr. We crop borders with respect to the scale factor for SR. All others are evaluated in RGB space without border crops.

### 4.1. Benchmark Evaluation

**Image Super-Resolution (SR)** In Tab.1, we perform a quantitative evaluation on image super-resolution by replacing the LayerNorm with our proposed *i*-LN in the

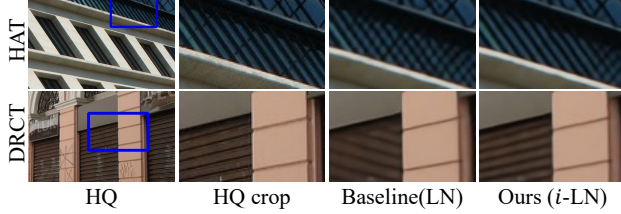


Figure 4. Quantitative results for  $\times 4$  super-resolution.

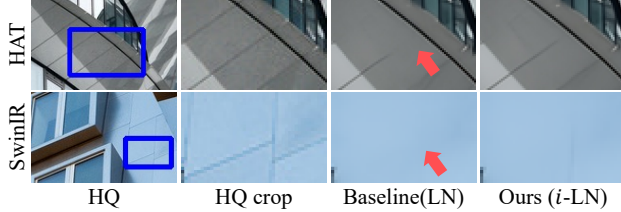


Figure 5. Quantitative results for denoising at noise level 25.

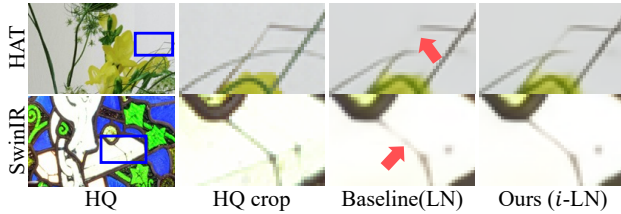


Figure 6. Quantitative results for JPEG compression artifact removal for quality factor 10.



Figure 7. Quantitative results for draining.

transformer-based SR methods: HAT [5], DRCT [11]. Compared to the conventional LayerNorm, our *i*-LN provides a significant performance gain in both PSNR and SSIM across all five datasets and all tested methods. In particular, for  $\times 2$  SR, the PSNR of our HAT + *i*-LN method surpasses HAT + LN by 1.16 dB on the Urban100 dataset and by 0.85 dB on the Manga109 dataset. We also provide visualization for super-resolution in Fig.4, validating that the proposed method predicts sharper textures with lesser artifacts.

**Image Denoising (DN)** We conduct color image denoising experiments by generating additive color Gaussian noise on benchmark datasets as CBSD68 [20], Kodak24 [10], McMaster [30], and Urban100 [12]. We replace LayerNorm in HAT and SwinIR with our proposed *i*-LN and evaluate both methods at noise levels 15 and 25. As shown in Tab.2, our *i*-LN achieves performance improvements across all datasets and noise levels. Notably, for the more challenging noise level of 25 on the Urban100 dataset, our HAT+*i*-LN

Backbone	$\sigma$	Urban100	CBSD68	Kodak24	McMaster
		PSNR	PSNR	PSNR	PSNR
HAT + LN [5]	15	35.489	34.285	35.347	35.440
HAT + <i>i</i> -LN (Ours)	15	<b>35.558</b>	<b>34.296</b>	<b>35.366</b>	<b>35.477</b>
SwinIR + LN [16]	15	35.077	34.164	35.147	35.183
SwinIR + <i>i</i> -LN (Ours)	15	<b>35.138</b>	<b>34.181</b>	<b>35.177</b>	<b>35.223</b>
HAT + LN [5]	25	33.296	31.622	32.864	33.105
HAT + <i>i</i> -LN (Ours)	25	<b>33.384</b>	<b>31.632</b>	<b>32.887</b>	<b>33.139</b>
SwinIR + LN [16]	25	32.753	31.480	32.643	32.829
SwinIR + <i>i</i> -LN (Ours)	25	<b>32.803</b>	<b>31.489</b>	<b>32.660</b>	<b>32.848</b>

Table 2. Quantitative comparison for **image denoising**. The best results are highlighted in **bold**.

Backbone	q	Urban100		LIVE1		Classic5	
		PSNR	SSIM	PSNR	SSIM	PSNR	SSIM
HAT + LN [5]	10	28.45	.8514	27.89	.8048	29.94	.8167
HAT + <i>i</i> -LN (Ours)	10	<b>28.52</b>	<b>.8530</b>	<b>27.90</b>	<b>.8057</b>	<b>29.96</b>	<b>.8178</b>
SwinIR + LN [16]	10	27.86	.8400	<b>27.65</b>	<b>.7995</b>	<b>29.72</b>	<b>.8111</b>
SwinIR + <i>i</i> -LN (Ours)	10	<b>27.92</b>	<b>.8410</b>	27.62	.7993	<b>29.72</b>	<b>.8111</b>
HAT + LN [5]	40	33.26	.9302	32.63	.9158	34.34	.9060
HAT + <i>i</i> -LN (Ours)	40	<b>33.36</b>	<b>.9312</b>	<b>32.67</b>	<b>.9162</b>	<b>34.39</b>	<b>.9066</b>
SwinIR + LN [16]	40	32.62	.9245	32.34	.9127	34.11	.9036
SwinIR + <i>i</i> -LN (Ours)	40	<b>32.68</b>	<b>.9252</b>	<b>32.35</b>	<b>.9129</b>	<b>34.12</b>	<b>.9038</b>

Table 3. Quantitative comparison for **JPEG compression artifact removal**. The best results for each setting are highlighted in **bold**.

Backbone	Train Dataset	Test100		Rain100L	
		PSNR	SSIM	PSNR	SSIM
HAT + LN [5]	Rain13K	29.52	.8905	34.35	.9471
HAT + <i>i</i> -LN (Ours)	Rain13K	<b>30.14</b>	<b>.9022</b>	<b>36.20</b>	<b>.9641</b>
SwinIR + LN [16]	Rain13K	27.45	.8766	33.00	.9434
SwinIR + <i>i</i> -LN (Ours)	Rain13K	<b>29.87</b>	<b>.8982</b>	<b>34.43</b>	<b>.9527</b>

Table 4. Quantitative comparison for **image deraining**. The best results are highlighted in **bold**.

improves the PSNR by 0.09 dB compared to HAT+LN. We also visualize denoising examples in Fig.5.

**JPEG compression artifact removal (CAR)** In Tab.3, we present quantitative results for JPEG compression artifact removal at quality 10 and 40, and evaluate them on Classic5 [9], LIVE1 [22], and Urban100 [12]. We compare the PSNR and SSIM scores between IR Transformers with either the vanilla LayerNorm or our tailored *i*-LN. Across all evaluated methods, our *i*-LN consistently outperforms the vanilla LayerNorm configuration. Examples of JPEG compression artifact removal are visualized in Fig.6.

**Image Deraining (DR)** We conduct experiments for the image deraining task for Test100 and Rain100L, and report PSNR, SSIM scores. As in Tab.4, our *i*-LN consistently outperforms the baseline LayerNorm, where we observe significant improvement of PSNR 2.42 dB on the Test100 dataset compared to SwinIR+LN. These consistent performance gains validate the broader applicability and robustness of our approach beyond typical IR tasks. We provide the visual examples in Fig.7.

Idx	Normalization Type	Spatially Consistent	Set5		Set14		BSD100		Urban100		Manga109	
			PSNR	SSIM								
1	LayerNorm	✗	32.51	.8992	28.79	.7876	27.68	.7411	26.55	.8015	31.01	.9150
2	LayerScale	✗	32.53	.8997	28.89	.7887	27.76	.7426	26.75	.8058	31.37	.9178
3	RMSNorm	✗	32.60	.9001	28.88	.7879	27.74	.7417	26.67	.8037	31.24	.9165
4	ReZero	✓	32.46	.8979	28.81	.7861	27.70	.7406	26.41	.7964	31.05	.9147
5	None	✓	32.57	.9001	28.95	.7898	27.79	.7437	26.86	.8088	31.54	.9198
6	InstanceNorm	✓	32.63	.9010	28.98	.7907	27.80	.7445	27.02	.8136	31.46	.9199
7	BatchNorm	✓	7.02	.0072	7.36	.008	7.39	.0074	7.17	.0079	6.57	.0078
8	BatchNorm <sup>†</sup>	✓	32.62	.9004	28.95	.7901	27.80	.7442	26.70	.8123	31.39	.9186
9	<i>i</i> -LN (Ours)	✓	<b>32.72</b>	<b>.9019</b>	<b>29.01</b>	<b>.7915</b>	<b>27.84</b>	<b>.7456</b>	<b>27.17</b>	<b>.8167</b>	<b>31.82</b>	<b>.9228</b>

Table 5. Quantitative comparison across different normalization strategies. † indicates evaluating in train-mode. Experiments were performed for the  $\times 4$  SR task with HAT. The best results are highlighted in **bold**.

## 4.2. Analysis

### 4.2.1. Channel Imbalance and Bias Alignment

Earlier, we observed extreme feature norms and significant imbalances in channel entropy, indicating highly peaky feature distributions concentrated in specific channels. Interestingly, despite these severe imbalances, baseline IR Transformers manage to converge and produce outputs with well-bounded images. This apparent paradox raises questions regarding internal mechanisms that enable these networks to remain effective despite such challenges. For closer inspection, we visualize the channel-axis unnormalized feature scale before the last normalization layer and the bias parameter of the normalization layer, across various IR tasks. As shown in Fig.9, we discovered that peaky patterns in the bias parameters, which precisely aligns with the channel index displaying extremely high feature magnitudes. Since these peaky feature magnitudes and biases exactly match, this provides a critical insight into the compensatory mechanisms that enable baseline models to produce ordinary scale outputs despite apparent internal discrepancies.

### 4.2.2. Comparison on Different Normalization Schemes

We analyze the effects of various normalization techniques, including representative normalization schemes as vanilla LayerNorm (LN), per-token RMSNorm (RMS), InstanceNorm (IN), BatchNorm (BN), our proposed *i*-LN. Considering previous studies where completely removing normalization from SR networks [18, 24] led to substantial performance improvements, we additionally tested a similar configuration, indicated as *None*, where we remove all the normalization layers in IR Transformers.

Additionally, we further investigate the empirical impacts of recent methods designed to stabilize Transformer training: ReZero (RZ) [3] and LayerScale (LS) [23]. ReZero removes LayerNorm from Transformer blocks and multiplies a learnable zero-initialized scalar to the residual path. Similarly, LayerScale multiplies a near-zero-

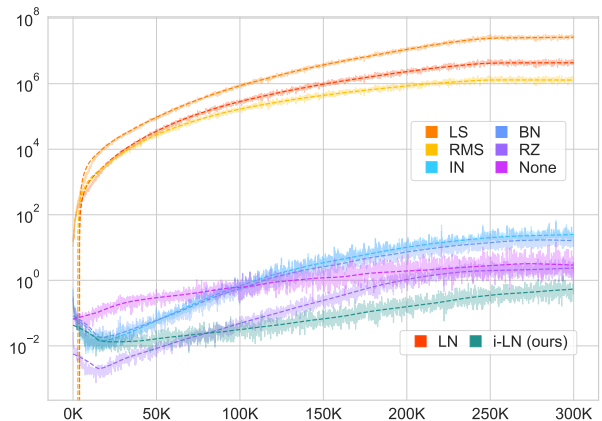


Figure 8. All per-token normalization schemes suffer from feature magnitude divergence, while feature magnitudes are well bounded in spatially holistic normalization methods.

initialized learnable diagonal matrix to the residual path but reintroduces LayerNorm. Since both methods initially multiply a (near) zero-scale factor to the network output, we consider them as potential solutions to resolve the feature divergence issue in IR tasks. Notably, these methods also align with prior studies in SR [18, 24], where multiplying a small scale factor to the residual path components significantly helped the network to converge.

Overall, this study aims to explore 1) the empirical impact of per-token normalization and compare it with various spatially holistic schemes, and 2) the following feature divergence phenomena of each, and also 3) determine which normalization method yields the best performance.

**Feature Divergence Analysis.** Fig.8 illustrates that feature divergence emerges always when using per-token normalizations: vanilla LN, RMSNorm, and LayerScale. In contrast, spatially consistent normalizations as our *i*-LN or BN, IN, and even the configuration without any normalization or ReZero do not exhibit the divergence trend. This observation aligns with our hypothesis that the feature divergence

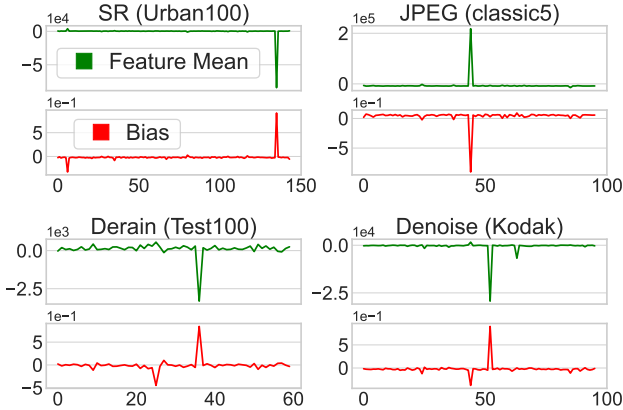


Figure 9. Bias parameters of the final normalization layer in IR Transformers using conventional (vanilla) LayerNorm, and corresponding unnormalized feature scales per channel. We observe exact alignment between peak channel indices in the normalization biases and those of the feature magnitudes, suggesting that these biases precisely counterbalance the extreme feature values across various IR tasks. This alignment reflects an internal compensatory mechanism enabling the model to produce stable outputs despite significant channel imbalances.

is mostly grounded in the per-token normalization and suggests that any spatially consistent normalization can significantly reduce this.

**Performance Comparisons.** We further analyze the empirical performance for each normalization scheme in Tab.5. Importantly, configurations employing spatially consistent normalization always outperform those with spatially *in*-consistent normalization.

Conventional LayerNorm performs the worst since per-token normalization disrupts spatial relationships and maps features into a unified normalized space, disregarding the input-dependent desirable feature statistics. In contrast, our *i*-LN achieves the best performance among all examined methods, demonstrating its effectiveness in preserving important spatial relationships and internal statistics.

Meanwhile, for the configurations without any normalization (None), a clear performance drop against our *i*-LN is observed due to potentially unstable gradients raised by the absence of normalization. Despite this, removal of the per-token normalization in this configuration yields both a well-bounded feature scale (Fig.8) and overall performance improvement compared to the vanilla LayerNorm. Similarly, InstanceNorm performs better than vanilla LayerNorm but worse than ours. The performance drop against ours is since it discards channel-wise information, which is critical for representing deep features. BatchNorm leads to a significant performance drop in eval-mode, despite healthy in train-mode; consistent with prior studies [18, 25].

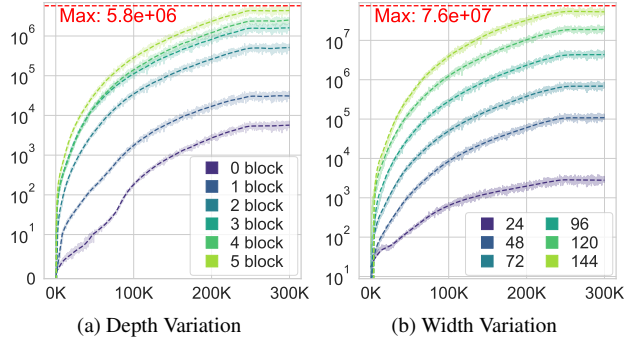


Figure 10. Feature divergence observed under a range of settings. We report squared mean of feature norms at the last building block by adjusting the following: (a) network depth, (b) network width,

Both LayerScale and RMSNorm show improvement against vanilla LN, but perform worse than methods with spatially consistent normalization. This is since they utilize the problematic per-token normalization scheme. ReZero fails to stabilize training, leading to a significant performance drop.

#### 4.2.3. Impact of Network Size

We investigate how the network size affects feature divergence. We gradually increase the depth and width of the IR Transformer and observe a clear positive correlation, as shown in Fig.10. This highlights that larger networks may be more susceptible to this issue. Meanwhile, prior analysis has shown that specific channels dominantly contribute to the abnormal feature statistics. This observation raises a concern that the effectiveness of *i*-LN could diminish as the network width is expanded. To test the robustness of *i*-LN, we increase the network’s width and accordingly, also the number of training iterations. We then compare the performance improvements between our method and the baseline. Tab.6 (Idx 1–3) indicates that *i*-LN not only retains its benefits but may also achieve greater performance gains in this expanded setting. This experiment suggests that feature divergence is an issue beyond mere capacity under-utilization.

#### 4.2.4. Empirical Study on Rescale

Although normalization stabilizes training, it can also remove critical input-dependent variations essential for accurate image reconstruction. We ablate the rescaling strategy and investigate its empirical effects. As shown in row 2–3 of Table 6, ablating the proposed rescaling leads to performance drop across multiple benchmarks. This supports the importance of effectively preserving important input-specific statistical features, enabling the network to gain flexibility when modeling intrinsic features. However, even when rescaling is omitted, we still outperform the baseline normalization in row 1 of Table 6 due to our spatially holistic normalization, which inherently preserves spatial corre-

Idx	Backbone	Quantization		Urban100	Manga109
1	HAT * + LN [5]	W	int8	26.8711	31.5266
2	HAT * + <i>i</i> -LN (Ours)	W	int8	27.5818	32.1657
3	HAT * + <i>i</i> -LN <sup>†</sup>	W	int4	25.0242	28.0831
4	HAT * + LN [5]	W	int4	26.8292	30.6596
5	HAT * + <i>i</i> -LN (Ours)	W+F	fp16	7.4640	5.0736
6	HAT * + LN [5]	W+F	fp16	27.5849	32.1693
7	HAT * + <i>i</i> -LN (Ours)	W+F	fp16	27.9034	32.0837
8	HAT * + LN [5]	W	int8	26.8711	31.5266
9	HAT * + <i>i</i> -LN (Ours)	W	int8	27.5818	32.1657
10	HAT * + LN [5]	W	int4	25.0242	28.0831
11	HAT * + <i>i</i> -LN (Ours)	W	int4	26.8292	30.6596
12	HAT * + LN [5]	W+F	fp16	7.4640	5.0736
13	HAT * + <i>i</i> -LN (Ours)	W+F	fp16	27.5849	32.1693

Table 6. We increase the dimension of the HAT model and train longer, indicated as HAT \*. *i*-LN<sup>†</sup> indicates our method without the rescaling strategy. PSNR results on Urban100 and Manga109 for  $\times 4$  SR under various quantization settings. Rows 4–7 apply weights-only (W) quantization, and rows 8–9 use half-precision for both weights and features (W+F fp16).

lations and stabilizes feature distributions more effectively than traditional per-token normalization schemes.

#### 4.2.5. Low Precision Inference

Image restoration networks often require deployment on lightweight edge devices, creating significant demand for efficient inference in IR Transformers. A common approach to enhance inference efficiency is reducing precision during model deployment. Consequently, we conducted experiments under reduced-precision inference conditions to empirically evaluate the effects of *i*-LN. Initially, we applied linear weight quantization to the model weights (Idx 4–7). As shown in Tab.6, vanilla LayerNorm resulted in substantial performance degradation, while *i*-LN demonstrated remarkable stability. We further conducted half-precision inference experiments, casting both internal feature values and weights to half-precision floating-point numbers (Idx 8–9). Fig.11 illustrates that vanilla LayerNorm generated extensive regions of black dots, indicating network-generated infinity values due to extreme internal feature magnitudes inadequate for low-precision conditions. Notably, for both the baseline and our method, no substantial performance degradation was observed in regions where the network maintained finite feature values. This highlights the necessity of well-bounded feature values achieved by *i*-LN, emphasizing its critical role in enabling efficient inference for IR Transformers.

#### 4.2.6. Enhanced Spatial Correlation via Structured RPE

Relative Position Embeddings (RPE) explicitly encodes relative spatial positions between tokens in an input-agnostic manner, similar to the convolution operation that inherently captures the spatial locality through their structured kernel patterns. Accordingly, we can consider well-structured RPEs as a strong indicator of enhanced spatial correlation understanding. In Fig.12, we analyze how our proposed

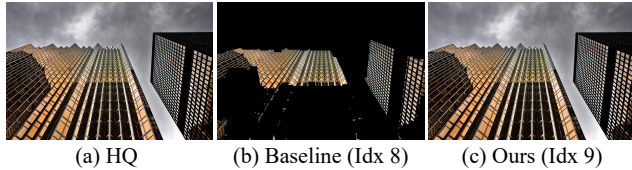


Figure 11. Half-precision inference result for  $\times 4$  SR. Each aligns to row 8–9 of Tab.6. The baseline shows noticeable artifacts.

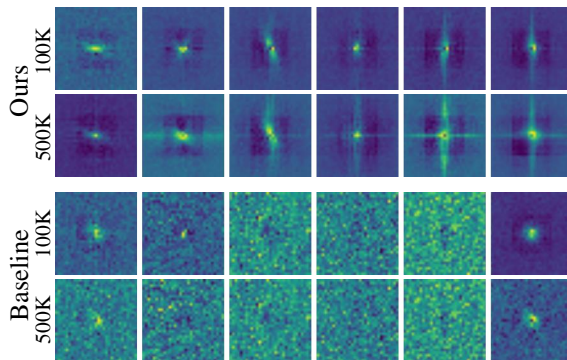


Figure 12. Visualization of Relative Position Embeddings (RPE). Ours exhibit well-structured RPEs, indicating the superiority in understanding the spatial relationship between pixels.

normalization method influences spatial relationship modeling by visualizing the learned RPE of both the baseline IR Transformer and our proposed method. The baseline IR Transformer exhibits noisy, unstructured embedding patterns, suggesting a limited capability to effectively model spatial correlations. Conversely, our method produces RPEs that resemble well-structured convolutional filter patterns, clearly indicating superior capture of spatial relationships. This structured embedding aligns with our hypothesis that our spatially holistic normalization better preserves intrinsic spatial correlations, thereby improving model convergence and restoration performance.

## 5. Conclusion

In this study, we addressed the critical issue of internal feature divergence observed in IR Transformers, primarily caused by LayerNorm. Our comprehensive analysis demonstrated that per-token normalization disrupts spatial correlations and induces unstable internal feature norms, significantly limiting the potential of Transformer-based image restoration models. To tackle these issues, we introduced the Image Restoration Transformer Tailored Layer Normalization (*i*-LN), which performs normalization across the entire spatio-channel dimension and incorporates an adaptive rescaling strategy to preserve input-specific feature statistics. Extensive experiments confirmed that our *i*-LN effectively stabilizes internal feature representations, preserves intrinsic spatial correlations, and significantly enhances restoration performance across various IR tasks.

## References

- [1] Eirikur Agustsson and Radu Timofte. Ntire 2017 challenge on single image super-resolution: Dataset and study. In *Proceedings of the IEEE Conference on Computer Vision and Pattern Recognition Workshops*, pages 126–135, 2017. 4
- [2] Jimmy Lei Ba, Jamie Ryan Kiros, and Geoffrey E Hinton. Layer normalization. *arXiv preprint arXiv:1607.06450*, 2016. 1
- [3] Thomas Bachlechner, Bodhisattwa Prasad Majumder, Henry Mao, Gary Cottrell, and Julian McAuley. Rezero is all you need: Fast convergence at large depth. In *Uncertainty in Artificial Intelligence*, pages 1352–1361. PMLR, 2021. 6
- [4] Marco Bevilacqua, Aline Roumy, Christine Guillemot, and Marie Line Alberi-Morel. Low-complexity single-image super-resolution based on nonnegative neighbor embedding. 2012. 4
- [5] Xiangyu Chen, Xintao Wang, Wenlong Zhang, Xiangtao Kong, Yu Qiao, Jiantao Zhou, and Chao Dong. Hat: Hybrid attention transformer for image restoration. *arXiv preprint arXiv:2309.05239*, 2023. 2, 4, 5, 8
- [6] Xiangyu Chen, Xintao Wang, Jiantao Zhou, Yu Qiao, and Chao Dong. Activating more pixels in image super-resolution transformer. In *Proceedings of the IEEE/CVF conference on computer vision and pattern recognition*, pages 22367–22377, 2023. 2
- [7] Xiangyu Chen, Zheyuan Li, Yuandong Pu, Yihao Liu, Jiantao Zhou, Yu Qiao, and Chao Dong. A comparative study of image restoration networks for general backbone network design. In *European Conference on Computer Vision*, pages 74–91. Springer, 2024. 4
- [8] Alexey Dosovitskiy, Lucas Beyer, Alexander Kolesnikov, Dirk Weissenborn, Xiaohua Zhai, Thomas Unterthiner, Mostafa Dehghani, Matthias Minderer, Georg Heigold, Sylvain Gelly, et al. An image is worth 16x16 words: Transformers for image recognition at scale. *arXiv preprint arXiv:2010.11929*, 2020. 1
- [9] Alessandro Foi, Vladimir Katkovnik, and Karen Egiazarian. Pointwise shape-adaptive dct for high-quality denoising and deblocking of grayscale and color images. *IEEE transactions on image processing*, 16(5):1395–1411, 2007. 4, 5
- [10] R. Franzen. Kodak lossless true color image suite. <http://r0k.us/graphics/kodak>, 1999. Volume 4, no. 2. 4, 5
- [11] Chih-Chung Hsu, Chia-Ming Lee, and Yi-Shiuan Chou. Drct: Saving image super-resolution away from information bottleneck. *arXiv preprint arXiv:2404.00722*, 2024. 3, 4, 5
- [12] Jia-Bin Huang, Abhishek Singh, and Narendra Ahuja. Single image super-resolution from transformed self-exemplars. In *Proceedings of the IEEE conference on computer vision and pattern recognition*, pages 5197–5206, 2015. 4, 5
- [13] Kui Jiang, Zhongyuan Wang, Peng Yi, Chen Chen, Baojin Huang, Yimin Luo, Jiayi Ma, and Junjun Jiang. Multi-scale progressive fusion network for single image deraining. In *Proceedings of the IEEE/CVF conference on computer vision and pattern recognition*, pages 8346–8355, 2020. 4
- [14] Tero Karras, Samuli Laine, Miika Aittala, Janne Hellsten, Jaakko Lehtinen, and Timo Aila. Analyzing and improving the image quality of stylegan. In *Proceedings of the IEEE/CVF conference on computer vision and pattern recognition*, pages 8110–8119, 2020. 3
- [15] Tero Karras, Miika Aittala, Jaakko Lehtinen, Janne Hellsten, Timo Aila, and Samuli Laine. Analyzing and improving the training dynamics of diffusion models. In *Proceedings of the IEEE/CVF Conference on Computer Vision and Pattern Recognition*, pages 24174–24184, 2024. 3
- [16] Jingyun Liang, Jiezhong Cao, Guolei Sun, Kai Zhang, Luc Van Gool, and Radu Timofte. Swinir: Image restoration using swin transformer. In *Proceedings of the IEEE/CVF International Conference on Computer Vision*, pages 1833–1844, 2021. 1, 2, 4, 5
- [17] Bee Lim, Sanghyun Son, Heewon Kim, Seungjun Nah, and Kyoung Mu Lee. Enhanced deep residual networks for single image super-resolution. In *The IEEE Conference on Computer Vision and Pattern Recognition (CVPR) Workshops*, 2017. 4
- [18] Bee Lim, Sanghyun Son, Heewon Kim, Seungjun Nah, and Kyoung Mu Lee. Enhanced deep residual networks for single image super-resolution. In *Proceedings of the IEEE conference on computer vision and pattern recognition workshops*, pages 136–144, 2017. 3, 4, 6, 7
- [19] Ze Liu, Yutong Lin, Yue Cao, Han Hu, Yixuan Wei, Zheng Zhang, Stephen Lin, and Baining Guo. Swin transformer: Hierarchical vision transformer using shifted windows. In *Proceedings of the IEEE/CVF international conference on computer vision*, pages 10012–10022, 2021. 2
- [20] David Martin, Charless Fowlkes, Doron Tal, and Jitendra Malik. A database of human segmented natural images and its application to evaluating segmentation algorithms and measuring ecological statistics. In *Proceedings Eighth IEEE International Conference on Computer Vision. ICCV 2001*, pages 416–423. IEEE, 2001. 4, 5
- [21] Yusuke Matsui, Kota Ito, Yuji Aramaki, Azuma Fujimoto, Toru Ogawa, Toshihiko Yamasaki, and Kiyoharu Aizawa. Sketch-based manga retrieval using manga109 dataset. *Multimedia Tools and Applications*, 76:21811–21838, 2017. 4
- [22] H Sheikh. Live image quality assessment database release 2. <http://live.ece.utexas.edu/research/quality>, 2005. 4, 5
- [23] Hugo Touvron, Matthieu Cord, Alexandre Sablayrolles, Gabriel Synnaeve, and Hervé Jégou. Going deeper with image transformers. In *Proceedings of the IEEE/CVF international conference on computer vision*, pages 32–42, 2021. 6
- [24] Xintao Wang, Ke Yu, Shixiang Wu, Jinjin Gu, Yihao Liu, Chao Dong, Yu Qiao, and Chen Change Loy. Esrgan: Enhanced super-resolution generative adversarial networks. In *Proceedings of the European conference on computer vision (ECCV) workshops*, pages 0–0, 2018. 3, 4, 6
- [25] Xintao Wang, Chao Dong, and Ying Shan. Reprsr: Training efficient vgg-style super-resolution networks with structural re-parameterization and batch normalization. In *Proceedings of the 30th acm international conference on multimedia*, pages 2556–2564, 2022. 3, 7
- [26] Wenhan Yang, Robby T Tan, Jiashi Feng, Jiaying Liu, Zongming Guo, and Shuicheng Yan. Deep joint rain detection and removal from a single image. In *Proceedings of the*

- IEEE conference on computer vision and pattern recognition*, pages 1357–1366, 2017. 4
- [27] Syed Waqas Zamir, Aditya Arora, Salman Khan, Munawar Hayat, Fahad Shahbaz Khan, and Ming-Hsuan Yang. Restormer: Efficient transformer for high-resolution image restoration. In *Proceedings of the IEEE/CVF conference on computer vision and pattern recognition*, pages 5728–5739, 2022. 2
- [28] Roman Zeyde, Michael Elad, and Matan Protter. On single image scale-up using sparse-representations. In *International conference on curves and surfaces*, pages 711–730. Springer, 2010. 4
- [29] He Zhang, Vishwanath Sindagi, and Vishal M Patel. Image de-raining using a conditional generative adversarial network. *IEEE transactions on circuits and systems for video technology*, 30(11):3943–3956, 2019. 4
- [30] Lei Zhang, Xiaolin Wu, Antoni Buades, and Xin Li. Color demosaicking by local directional interpolation and nonlocal adaptive thresholding. *Journal of Electronic imaging*, 20(2): 023016–023016, 2011. 4, 5